A genetically encoded calcium indicator for chronic *in vivo* two-photon imaging

Marco Mank[1], Alexandre Ferrão Santos[1], Stephan Direnberger[1], Thomas D Mrsic-Flogel[1,3], Sonja B Hofer[1,3], Valentin Stein[1], Thomas Hendel[1], Dierk F Reiff[1], Christiaan Levelt[2], Alexander Borst[1], Tobias Bonhoeffer[1], Mark Hübener[1] & Oliver Griesbeck[1]

Neurons in the nervous system can change their functional properties over time. At present, there are no techniques that allow reliable monitoring of changes within identified neurons over repeated experimental sessions. We increased the signal strength of troponin C–based calcium biosensors in the low-calcium regime by mutagenesis and domain rearrangement within the troponin C calcium binding moiety to generate the indicator TN-XXL. Using *in vivo* two-photon ratiometric imaging, we show that TN-XXL exhibits enhanced fluorescence changes in neurons of flies and mice. TN-XXL could be used to obtain tuning curves of orientation-selective neurons in mouse visual cortex measured repeatedly over days and weeks. Thus, the genetically encoded calcium indicator TN-XXL allows repeated imaging of response properties from individual, identified neurons *in vivo*, which will be crucial for gaining new insights into cellular mechanisms of plasticity, regeneration and disease.

Modern *in vivo* imaging technology in living brains has become invaluable in the study of neuronal networks as they process sensory information. It usually relies on the combination of non-linear microscopy and the use of fluorescent contrast labels[1]. In particular, imaging of fluorescent calcium indicators has been used for noninvasive, real-time measurement of spiking activity of individual neurons and neural populations *in vivo*[2–6]. Neuronal circuits involved in sensory information processing mature during development and adapt in response to experience[7,8]. Calcium dye leakage from neurons during longer recording sessions and the failure to repeatedly load new indicator into neuronal tissue[6,9] has prohibited long-term imaging of such processes over days and weeks. Implanted microelectrodes allow recordings from individual neurons over periods of up to three weeks[10], but simultaneous sampling of many cells and knowledge of their precise location in the cortex is impossible. Thus, current technical limitations restrict our ability to follow the responses of identified neurons *in vivo* over consecutive recording sessions.

Genetically encoded calcium sensors, which have become an alternative to synthetic indicator dyes in many applications[11,12],

could solve this problem. Genetically encoded calcium indicators are solely composed of amino acids, form spontaneously within cells after onset of expression and, unless specific targeting sequences are used, localize reliably to the cytosol without segregation into organelles or leakage from expressing cells. Their usefulness for the detection of subtle sensory-evoked calcium signals *in vivo*, however, has been limited because of smaller signal strength at lower calcium concentrations and/or lower brightness compared to some of the best synthetic dyes[13–15]. We recently generated a family of calcium biosensors based on the calcium binding protein troponin C (TnC) from skeletal and cardiac muscle[16,17]. Transgenic expression in the mouse brain demonstrated stable expression and full functionality of a slightly modified version of the first-generation sensor TN-L15 (ref. 18). We now have rearranged the calcium sensing moiety TnC within the indicator and performed mutagenesis of selected amino acid residues within chicken skeletal muscle TnC to increase overall signal strength and sensitivity in the regime of physiologically relevant calcium concentrations. These efforts have led to the new indicator TN-XXL. We show that TN-XXL is functional *in vivo* in flies and mice, giving reliable signals in response to small changes in electrical activity. Using *in vivo* two-photon ratiometric imaging, we demonstrate that TN-XXL can be used to obtain tuning curves of orientation-selective neurons in visual cortex. Moreover, TN-XXL allows the repeated recording of sensory-evoked activity from the same individual neurons in mouse visual cortex during consecutive imaging sessions over days and weeks.

RESULTS
Generation and characterization of TN-XXL
For a better resolution of physiologically relevant subtle calcium signals, we aimed to increase signal strength of TnC-based sensors in the range of 100–500 nM free calcium. As a starting point for our engineering, we used the indicator TN-XL (ref. 17), which showed high FRET change, fast kinetics and high selectivity for calcium over magnesium. Because of its intermediate calcium affinity ($K_d = 2.2$ μM), it is more suitable for subcellular tagging to

Figure 1 | Generation and *in vitro* characterization of TN-XXL. (**a**) Schematic representation of domain rearrangement and mutagenesis used to develop TN-XXL. The indicator is drawn as a linear sequence with four loops with roman numerals indicating EF hands I–IV of chicken skeletal muscle troponin C (csTnC). Blue and yellow lines at N- and C-terminal positions represent the fusion of CFP and Citrine cp174 to csTnC. Amino acid residues determined to be optimal as start and end points for domain doubling (Ser94 and Gln162), mutations within EF hand III to abolish magnesium binding (mutations N108D and D110N) and one helix-stabilizing mutation to increase calcium affinity of the C-terminal lobe (I130T) are indicated. All numbering of amino acid residues refers to the wild-type sequence of csTnC. Domain rearrangement involved the deletion of the N-terminal lobe (gray line) of csTnC, containing EF hands I and II (middle row), and the doubling, connected by means of a short linker (orange, bottom row), of the C-terminal lobe (black line) between Ser94 and Gln162. (**b**) Calcium titration of TN-XXL, TN-L15 and TN-XL. The resulting K_d values are 710 nM (TN-L15), 2.2 μM (TN-XL) and 800 nM (TN-XXL) ($n = 4$; error bars, mean ± s.d.). (**c**) Corresponding signal strengths (in $\Delta R/R$ (%)) ($n = 4$; mean ± s.d.) of the three biosensors given as a function of free calcium *in vitro*. $\Delta R/R$ values are calculated according to the peak values of donor (475 nm) and acceptor (527 nm) fluorescence and the ratio obtained at 0 nM free calcium.
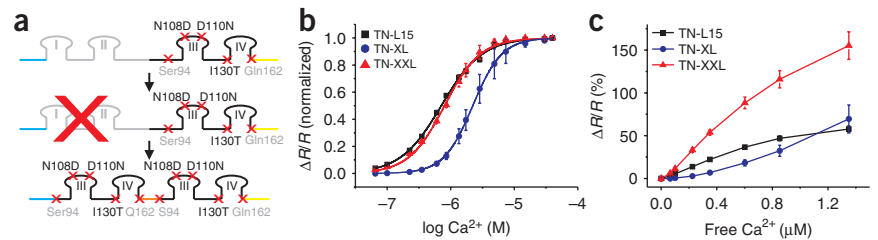
structures expected to encounter large calcium fluctuations than to detecting small cytosolic rises in free calcium. To shift the sensitivity of TN-XL in the required direction, we rearranged the domains of TnC. TnC, like calmodulin, is a protein in which two lobular domains are linked by a connecting helix. The N- and C-terminal lobes in these proteins differ in calcium-binding properties and can exert different, independent sensor functions[19–21]. The lower-affinity N-terminal lobe of TnC is considered the essential regulator of muscle contraction, whereas the high-affinity Ca^{2+}/Mg^{2+} binding C-terminal lobe is considered to possess a structural function[20]. We reasoned that single-domain sensors containing only the C-terminal lobe of TnC would show increased calcium sensitivity. We therefore deleted the N-terminal lobe of TnC and tested various N- and C-terminal deletions of the remaining C-terminal lobe to try to further amplify the sensor response to calcium (**Fig. 1a**). The best-working C-terminal domain started with Ser94 and ended at Gln162. Unfortunately, sensors with single lobes showed high FRET under basal conditions and only small

calcium-induced FRET changes. We therefore concatenated two C-terminal lobes with a central linker. Several amino acid changes enhanced performance of the resulting sensor, mainly the mutations N108D and D110N (ref. 17) to block magnesium-induced conformational change, which largely operates through EF hand III. We also introduced the mutation I130T (ref. 22), which exerts stabilizing effects on the incoming helix of EF hand IV and was previously found to significantly increase TN-XL sensor affinity[17]. We named the resulting improved calcium sensor TN-XXL.

We compared the calcium response of TN-XXL to the previously described TnC-based calcium sensor proteins TN-L15 (ref. 16) and TN-XL (ref. 17) using normalized calcium titration curves (**Fig. 1b**). TN-XXL had a K_d of 800 nM and a Hill coefficient of

Figure 2 | *In vivo* two-photon imaging and calibration of TN-XXL in *Drosophila* motor neuron boutons. (**a**) Bright-field image of a filet preparation of a *Drosophila* larva. Scale bar, 1 mm. (**b**) Same field of view taken by epifluorescence excitation. Pan-neuronal TN-XXL expression fluorescently labels the entire nervous system: brain (b), ventral nerve cord (v), and nerves innervating individual body segments (sn). (**c**) Close-up on larval body wall muscle 6/7 (m), exemplifying the recording situation in a rostral abdominal segment. The cut end of the intersegmental nerve (sn) was placed in a suction electrode (el) for electrical stimulation of presynaptic motor neuron endings. Scale bar, 50 μm. (**d**) Two-photon excitation of TN-XXL fluorescence at a neuromuscular junction on muscle 6/7 (collapsed image stack taken by two-photon microscopy). Axons and type Is and Ib boutons are labeled by bright TN-XXL fluorescence. In contrast, there is no fluorescence signal detectable from the muscles. Scale bar, 10 μm. (**e,f**) Two-photon excitation and close-up on two presynaptic boutons, marked by the red box in **d**, showing CFP fluorescence (**e**) and simultaneously imaged Citrine cp174 (**f**). Scale bars, 5 μm. (**g**) TN-XXL fluorescence changes in presynaptic boutons increase with action potential frequency (0–160 Hz, 2 s; black stimulus bar). Fractional fluorescence changes of the Citrine cp174/CFP ratio ($\Delta R/R$) are plotted as a function of time. (**h–j**) Comparison of $\Delta R/R$ in three different TnC-based calcium indicators: TN-L15, TN-XL and the new TN-XXL. (**h**) Maximum $\Delta R/R$ at steady state plotted as a function of $\Delta[Ca^{2+}]_i$ (action potential frequency was translated into $\Delta[Ca^{2+}]_i$ per ref. 23). (**i,j**) $\Delta R/R$ plotted as a function of time at 10 Hz (**i**) and 20 Hz (**j**) stimulation. Genotype: $elav^{C155}$-GAL4/$elav^{C155}$-GAL4; UAS-TN-XXL/UAS-TN-XXL. Sample sizes: $52 < n < 60$ type Ib boutons.
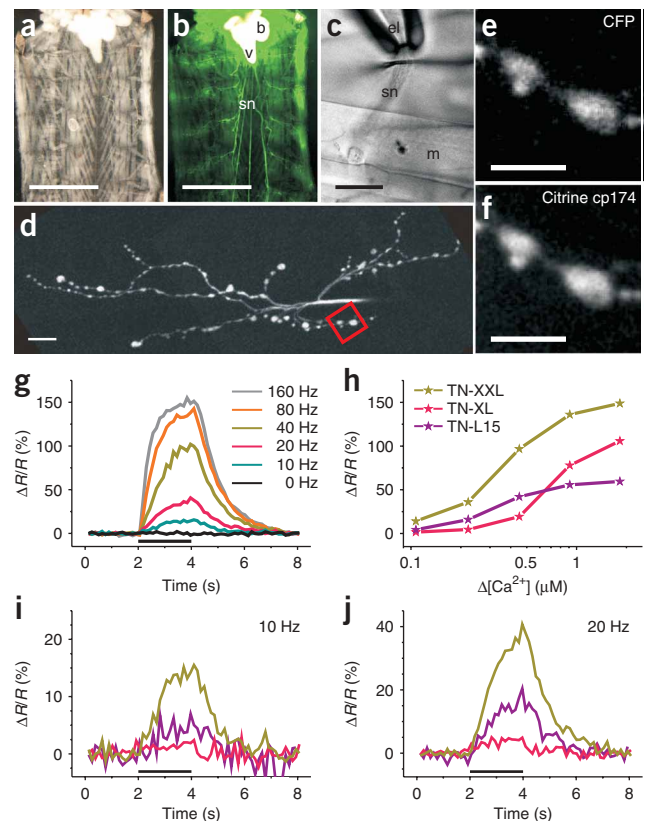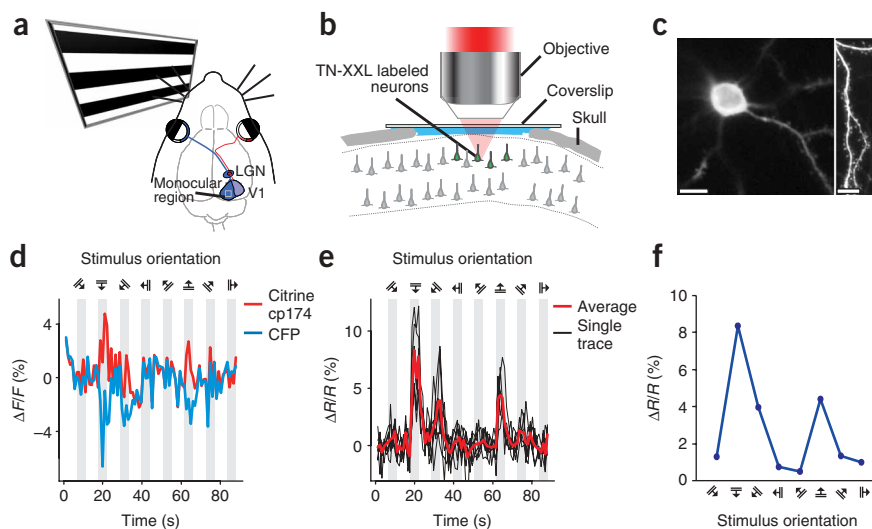
Figure 3 | Imaging stimulus-evoked TN-XXL signals in mouse visual cortex. (**a**) Schematic of the mouse visual system and stimulus presentation. Moving gratings of different orientations were displayed on a screen in front of the mouse, contralateral to the imaged visual cortex. (**b**) Schematic of experimental approach for *in vivo* two-photon imaging from mouse visual cortex. (**c**) Left, *in vivo* two-photon image of a recombinant SFV–infected pyramidal neuron expressing TN-XXL (average of 200 frames), 275 μm below the cortical surface. Right, dendrites and spines from this cell at a depth 120 μm. Scale bars, 10 μm. (**d**) Average (six trials) change in fluorescence ($\Delta F/F$) of Citrine cp174 and CFP during visual stimulation (gray bars). Stimulus orientation and direction are indicated by the symbols at the top. Note opposite sign of signal change in both channels during stimulation with horizontal gratings. (**e**) Average and single-trial responses of the ratiometric signal ($\Delta R/R$). (**f**) Orientation tuning curve of the imaged neuron.

1.5. For a better comparison, we plotted the actual signal $\Delta R/R$ (the fractional ratio change in percent) of all three sensors in the range from 0 to 1.4 μM free calcium (**Fig. 1c**).

We also applied this doubling strategy to a variety of skeletal TnCs of different species. For that purpose we used chicken skeletal TnC, mouse skeletal TnC and zebrafish skeletal TnC (**Supplementary Fig. 1** online). In mouse TnC and zebrafish TnC we introduced the mutations N105D and D107N to gain the same blockage of magnesium-induced conformational change in the corresponding loop of EF III. Of the nine possible lobe combinations, only chicken TnC C-lobe + mouse TnC C-lobe and zebrafish TnC + chicken TnC showed roughly the same signal strength as TN-XXL in the lower-calcium regime. Although not of immediate advantage in the present study, this homology-driven combinatorial approach promises to be a valuable strategy for further biosensor engineering.

To characterize the response properties of TN-XXL in living neurons we generated recombinant Semliki Forest virus vectors (SFV) to deliver TN-XXL into organotypic hippocampal slices. Action potentials were generated in the somata of whole-cell patched infected CA1 neurons and indicator fluorescence was monitored by ratiometric CCD camera imaging. Series of current-triggered action potential trains of 1, 2, 5, 10 and 20 action potentials were elicited at a stimulation frequency of 20 Hz (current pulses: 0.2–0.4 nA for 10 ms) (**Supplementary Fig. 2**, **Supplementary Methods** online). The average $\Delta R/R$ of four CA1 neurons showed maximal ratio changes ($\Delta R/R_{max}$) for one action potential of 1.6% ± 0.3, two action potentials of 2.8% ± 0.5, five action potentials of 5.9% ± 1.1, ten action potentials of 8.9% ± 1.4 and 20 action potential of 11.2% ± 1.6 (**Supplementary Fig. 2b**). The response kinetics of the sensor were much slower than the kinetics

of individual action potentials and comparable to those of previous TnC-based calcium sensor proteins. To determine whether the measured ratio change was a reliable FRET signal, the fluorescence intensity change $\Delta F/F$ of the cyan fluorescent protein (CFP) and Citrine cp174 (ref. 17) channels was evaluated. For the CFP channel, an apparent decrease of the fluorescence intensity could be observed, as well as an increase of intensity in the Citrine channel. Even for a single current pulse evoking one action potential, a signal was observed (**Supplementary Fig. 2**).

Calibration of TN-XXL fluorescence changes in neurons *in vivo*

We generated TN-XXL–expressing flies (**Fig. 2a,b**) and used presynaptic boutons of the *Drosophila melanogaster* neuromuscular junction (NMJ) as an *in vivo* testing ground[12,14] to cross-calibrate fluorescence changes of TN-XXL to changes in neural activity and free intracellular calcium. Known changes in intracellular free calcium[23] were induced by eliciting action potential trains (**Fig. 2c**) at different frequencies (0–160 Hz). This protocol results in a frequency-dependent, linear increase in intracellular calcium concentration $\Delta[Ca^{2+}]_i$ up to 1.83 μM at 160 Hz superimposed on a free cytosolic calcium concentration at rest $[Ca^{2+}]_{rest}$ of 31 nM at 0 Hz (ref. 23). The changes in fluorescence of TN-XXL within presynaptic boutons (**Fig. 2d**) were imaged by two-photon laser scanning microscopy with simultaneous recording of both emission wavelengths (**Fig. 2e–g**). We also compared $\Delta R/R$ of TN-XXL to TN-L15 and TN-XL. However, only TN-XXL reported sustained neural activity of 10 Hz for 2 s, corresponding to $\Delta[Ca^{2+}]_i$ of ~100 nM, with a signal to noise ratio > 2 (**Fig. 2h–j**). Well above 40 Hz (corresponding to ~500 nM $\Delta[Ca^{2+}]_i$), TN-XXL signals began to saturate, and
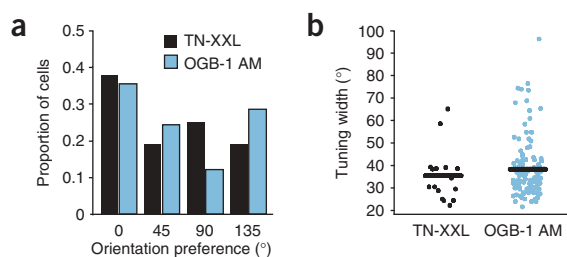

Figure 4 | Comparison of responses to drifting grating stimuli in neurons expressing TN-XXL and OGB-1 AM. (**a**) The distribution of preferred orientations for responsive neurons. For example, a preferred angle of 0° indicates that a neuron responded most vigorously to a horizontal grating drifting in an upward or downward direction. Each category (0°, 45°, 90°, 135°) includes neurons which were tuned to orientations ± 25° from the stated value. Note the bias for horizontal (0°) gratings in both TN-XXL and OGB-1 AM neurons. (**b**) The distribution of the width of orientation tuning. Each value represents the half-width at half-maximum response of fitted tuning curves. Horizontal lines indicate mean values.

ultimately a maximum fluorescence change of 150% $\Delta R/R$ was reached. Time constants of the fluorescence change shown at 40 Hz at 20–23 °C were 1.04 s for the rise and 0.88 s for the decay.

Compared to the other indicators, TN-XXL (**Fig. 2h**) showed higher $\Delta R/R$ over the entire range of $\Delta[Ca^{2+}]_i$ (0.1–1.8 μM), in good agreement with the *in vitro* titration data (**Fig. 1b,c**). These improvements are most obvious when TN-XXL fluorescence changes at 10 and 20 Hz, corresponding to $\Delta[Ca^{2+}]_i$ of only 0.1 μM and 0.2 μM, are compared to $\Delta R/R$ of its congener indicators (**Fig. 2i,j**). Hence, our recordings from small subcellular compartments of individually identifiable neurons suggest that TN-XXL can discern meaningful biological signals and low rates of neuronal activity from noise in a variety of different preparations and experiments *in vivo*.
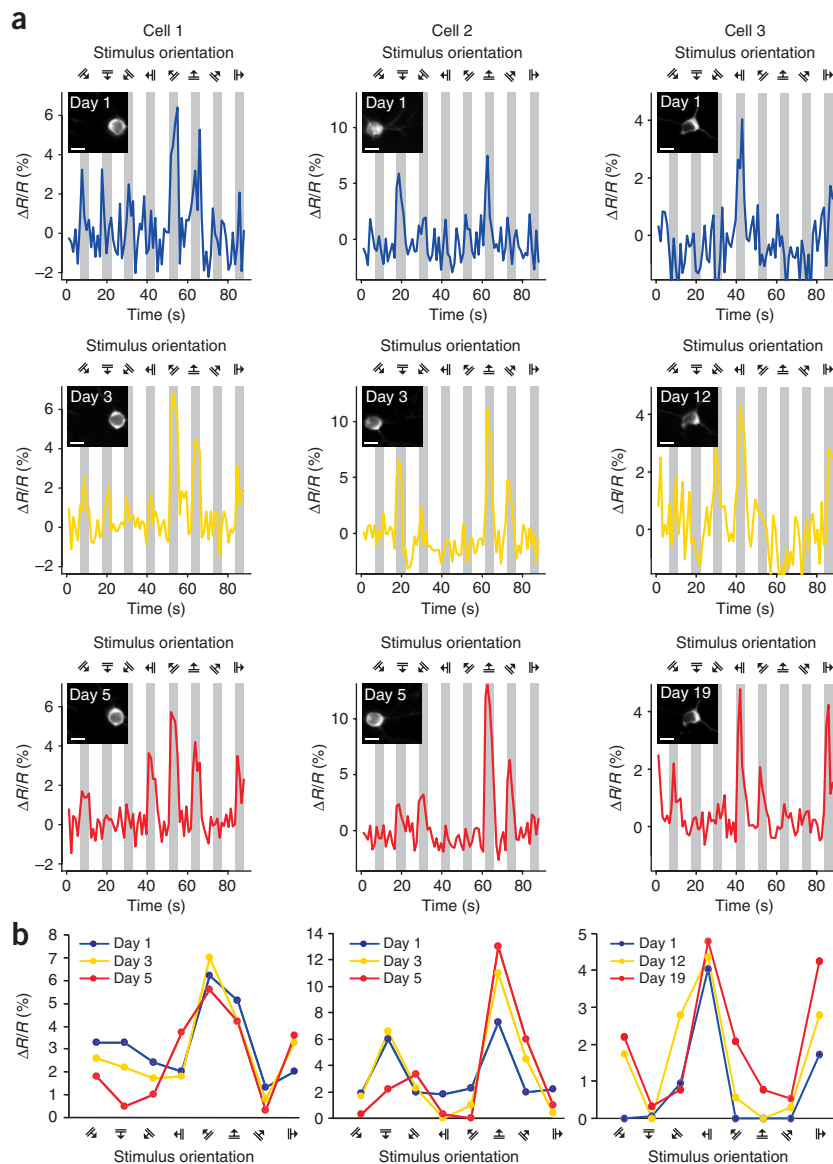
Imaging stimulus-evoked activity in mouse visual cortex

To test TN-XXL in the mammalian brain, we induced its expression in the upper layers of the visual cortex either by *in utero* electroporation at embryonic day 14–16 (resulting in expression in excitatory neurons only) or by injection of recombinant SFV. SFV infected both neurons and astrocytes, and we selected anatomically identified pyramidal neurons for analysis (**Fig. 3**). Expression levels typically were high, allowing the visualization of subcellular structures such as dendritic spines (**Fig. 3c**). Photobleaching was negligible, such that the same cell could be repeatedly imaged over hours. To measure stimulus-evoked responses of individual neurons in the visual cortex, we presented whole-field drifting grating stimuli of eight different directions to the mouse (**Fig. 3a**). For each acquired frame, fluorescence intensities in both channels were determined in a region of interest encompassing a single cell body, and relative changes ($\Delta F/F$) were computed using the average of the three frames preceding stimulus movement as baseline. Stimulus-locked fluorescence changes of opposite sign could be detected in both channels, with donor fluorescence decreasing and acceptor fluorescence increasing (**Fig. 3d**). A marked increase in signal-to-noise ratio was achieved by computing the ratio between the two channels (**Fig. 3e**). Changes in $\Delta R/R$ were clearly visible at the single-trial level; they were robust and reproducible, and allowed us to construct orientation tuning curves from individual imaged neurons (**Fig. 3f**).

Comparison of OGB-1 and TN-XXL

We compared TN-XXL performance to the synthetic calcium indicator dye Oregon Green BAPTA-1 acetoxymethyl (AM) ester (OGB-1 AM). Although the stimulus-evoked peak fluorescence signals were larger for OGB-1 AM–labeled neurons (for OGB-1 AM, $16.7 \pm 7.5\%$ $\Delta F/F$, $n = 780$; for TN-XXL, $7.4 \pm 5.6\%$ $\Delta R/R$, $n = 16$, mean $\pm$ s.d.), response profiles were comparable for both indicators (**Supplementary Fig. 3** online). However, the proportions of responsive neurons were different for the two indicators. With OGB-1 AM, 63% of labeled cells (780 of 1,244 neurons) responded significantly (analysis of variance, $P < 0.01$) to drifting gratings, but only 22% of TN-XXL–expressing neurons (16 of 72 neurons) did so. The distribution of preferred orientations was similar for both sensors (**Fig. 4a**), showing a bias toward horizontally oriented bars, which is typical of the mouse visual cortex[24]. Moreover, the width of tuning for responsive TN-XXL–expressing neurons was not significantly different from responsive OGB-1 AM labeled cells (**Fig. 4b**; tuning width for OGB-1 AM $38.42° \pm 12.86°$, $n = 780$; for TN-XXL,

Figure 5 | Repeated imaging of sensory-evoked calcium signals using TN-XXL. (**a**) Visually evoked calcium transients imaged in three *in utero*–electroporated, TN-XXL–expressing neurons at successive time points (averages of 6 trials for cells 1 and 2 at all time points; averages of 15, 10 and 35 trials for cell 3 on days 1, 12 and 19, respectively). Scale bar, 10 μm. (**b**) Orientation tuning curves from neurons in **a** obtained on different days after start of the experiment. Note stable tuning over time in all cells.

35.13° ± 11.83°, $n = 16$, mean ± s.d., $P = 0.31$, Wilcoxon rank sum test). Together, these data indicate that the tuning properties of responsive cortical area V1 neurons can be faithfully measured with the genetically encoded calcium indicator TN-XXL.

Chronic *in vivo* calcium imaging

Although SFV infection of neurons in the visual cortex allowed us to rapidly test TN-XXL function *in vivo*, long-term expression is not possible with this virus because of cytotoxicity. In contrast, stable expression of TN-XXL was possible with *in utero* electroporation, allowing us to repeatedly monitor the response properties of single neurons over extended periods of time in mice implanted with a cranial window[25]. Individual TN-XXL–expressing neurons were imaged and screened for orientation-selective responses in the first imaging session; their positions were retrieved in subsequent experiments using superficial blood vessels as landmarks. Neurons imaged several times over periods of up to 3 weeks did not show any apparent changes to their somatic morphology (**Fig. 5a**, insets), suggesting that repeated imaging did not cause photodamage. Notably, we detected clear, stimulus-driven calcium responses in the same neurons over the course of several days and weeks (**Fig. 5a**). Although there was some variation in peak response amplitudes between sessions (likely caused by differences in the depth of anesthesia from session to session), stimulus selectivity remained highly stable over time (**Fig. 5b**). The overall shape of the tuning curves was similar between sessions and preferred orientation did not change. We did note that the directional selectivity of some neurons varied over time, which might, however, also reflect varying depths of anesthesia over experiments[26].

DISCUSSION

The development of two-photon laser microscopy combined with the use of calcium-sensitive dyes has greatly improved the study of *in vivo* neural activity at the single-cell level[2–6]. Nevertheless, the failure to chronically label neurons with calcium-sensitive dyes[6,9] has so far prevented their use for monitoring long-term functional changes in the intact brain. Such chronic recordings of single-cell activity are crucial for a full understanding of how individual neurons change their functional properties during development and learning or as a consequence of a disease process. At present, the only method for repeatedly recording single cell activity *in vivo* is by means of chronically implanted electrodes[10]. Although this approach in principle enables recording of a cortical region over a period of months, cell death and gliosis at the electrode tips often degrade the recording quality over time, and electrode drift demands the use of corrective algorithms to track single neurons and to disentangle smeared spike clusters[27]. Even under optimal conditions, there is always some uncertainty as to whether a chronic recording is from the same neuron, if the only criteria for identifying a cell are spike waveform and neuronal tuning. Imaging solves this problem, since the characteristic morphology of neurons and their location relative to other cellular elements allows for unequivocal identification of a cell.

Our experiments show that TN-XXL is well suited for long-term functional imaging. TN-XXL–expressing neurons had orientation tuning curves indistinguishable from OGB-1 AM–labeled cells, indicating that TN-XXL allowed for the reliable determination of neuronal response characteristics. However, in comparison to OGB-1 AM, fewer TN-XXL–expressing cells responded

significantly to drifting grating stimuli (22%). Although this might be partially due to the lower signal amplitudes of TN-XXL compared to OGB-1 AM, potential neuropil contamination of somatic signals in tissue bulk-loaded with synthetic indicators[1] may increase the apparent number of responsive neurons. In contrast, under conditions of sparse labeling with TN-XXL (as used here), the neuropil does not show any response (data not shown). Nonetheless, the fraction of 22% visually responsive neurons with TN-XXL is likely an underestimate of the true proportion of responsive cells. Future improvements of the sensor are thus desirable.

Chronic recordings from awake, behaving animals should become feasible by combining the use of TN-XXL with head-mounted two-photon imaging devices[9,28]. Inevitable brain motion artifacts during imaging in awake animals[9] can be alleviated with ratiometric indicators such as TN-XXL because movement-induced, correlated changes in both fluorescent channels are cancelled out (**Fig. 3**). We have previously demonstrated that it is possible to express fully functional TnC-based calcium sensors transgenically in the mouse brain throughout the lifetime of the animal[18]. Given the stability of the cranial window preparation, the time span for chronic imaging can therefore be greatly expanded, since neurons expressing TnC-based sensors over months appeared structurally and functionally normal. Finally, apart from applications in neuroscience such as described here, we see many interesting possibilities for using chronic *in vivo* calcium imaging in clinically relevant settings—for example, when following the progress of a disease process or monitoring effects of drug applications in identified cells over weeks or months.

METHODS

Cranial implant surgery and virus injection in mice. All experimental procedures were carried out in compliance with institutional guidelines of the Max-Planck-Gesellschaft, the local government (Regierung von Oberbayern) and the institutional animal care and use committee of the Royal Netherlands Academy of Arts and Sciences. C57BL/6 mice (postnatal days 28–32) were anesthetized with a mixture of fentanyl (Hexal, 0.05 mg per kilogram body weight), midazolam (Roche, 5.0 mg/kg) and medetomidin (Pfizer, 0.5 mg/kg). Eye cream (Isopto-max, Alcon) was applied to prevent dehydration during surgery. A 5-mm craniotomy was carried out above the visual cortex as determined by stereotaxic coordinates. The exposed cortical surface was kept moist with cortex buffer (125 mM NaCl, 5 mM KCl, 10 mM glucose, 10 mM HEPES buffer, 2 mM MgSO$_4$ and 2 mM CaCl$_2$, pH 7.4). The SFV TN-XXL solution (0.5 μl) was gradually (3 min) pressure injected (0.8 p.s.i.) in the visual cortex at a depth of 50–300 μm with a borosilicate glass micropipette (Harvard Apparatus GC150F-10). After viral injection the cortex was sealed with 1.25% agarose in cortex buffer and a coverslip. Dental acrylic cement (Palladur, Heraeus Kulzer) was used to seal the coverslip and mount a removable head bar on the skull to immobilize it during imaging.

Two-photon imaging in mice. Activity of cortical neurons was monitored by imaging fluorescence changes with a custom-built microscope and a mode-locked Ti:sapphire laser (Mai Tai, Spectra-Physics) at 830 nm (OGB-1 AM) or 860 nm (TN-XXL) through a ×40 water-immersion objective (0.8 numerical

aperture, Olympus). The two-photon excitation cross-sections of CFP and yellow fluorescent protein (YFP) variants such as Citrine are well known[29], and relatively specific excitation of CFP over YFP can be obtained at wavelengths from 800–860 nm. Excitation at 860 nm *in vivo* yielded slightly larger responses from neurons in mouse visual cortex than excitation at 830 nm. For TN-XXL, emitted fluorescence was passed through a long-pass dichroic mirror (505 nm) and bandpass filters (CFP: peak 480 nm, bandwidth 40 nm; Citrine cp174: peak 535 nm, bandwidth 30 nm). Scanning and image acquisition were controlled by Fluoview software (Olympus). The average power delivered to the brain was < 50 mW.

Visual stimulation and data acquisition. Mice were anesthetized with a mixture of Fentanyl (0.05 mg/kg), Midazolam (5.0 mg/kg) and Medetomidin (0.5 mg/kg). Anesthesia was maintained by reinjecting one-third of the initial dose approximately every hour. Neuronal responses to visual stimulation were assessed using grating stimuli presented on a monitor in front of the mouse. Image (512 × 512 pixels) sequences were acquired at 1.1 s per frame. Stimuli consisted of high-contrast square-wave gratings presented at four orientations and in both directions. Each individual stimulus cycle consisted of 6.6 s of stationary grating, followed by 4.4 s of drift. This standing-moving sequence was used to avoid unwanted stimulus-on responses during the data acquisition period. Image sequences were aligned for tangential drift and analyzed with custom programs written in ImageJ (US National Institutes of Health), R (http://www.R-project.org/) and Matlab (Mathworks). Recordings with significant brain movements, vertical drift, or both were excluded from further analysis. Cell outlines were detected using a semiautomated algorithm based on morphological measurements of cell intensity, size and shape and subsequently confirmed by visual inspection. All pixels within a cell's outline were averaged to give a single time course ($\Delta F/F$ or $\Delta R/R$). Response amplitude was calculated from the averages of at least five stimulus repetitions, as the average $\Delta F/F$ or $\Delta R/R$ of the three 1.1-s frames immediately after stimulus onset, centered around the stimulus-evoked response maximum. The baseline was computed as the mean $\Delta F/F$ or $\Delta R/R$ of the three frames immediately before stimulus onset. Cells were considered visually responsive if the response to any of the stimuli was significantly different from the baseline (analysis of variance, $P < 0.01$). Preferred orientation was obtained by vector averaging. For quantitative analysis, tuning curves were fitted with the sum of two circular gaussian functions (von Mises distribution: $A \exp\{-k [1 - \cos(j - j_0)]\}$) (ref. 30). Tuning width is the half-width at half-maximum of these fits. OGB-1 AM responses were obtained from the binocular region of mouse visual cortex, which receives input from both eyes. TN-XXL responses were obtained from cells located in both monocular and binocular cortex (**Fig. 3a**). In both cases, responses were elicited by presenting gratings to the contralateral eye only. To ensure that the quantification and comparison of visually evoked responses in neurons labeled with OGB-1 AM and TN-XXL was comparable, we included only those OGB-1 AM neurons that were driven predominantly or exclusively by the contralateral eye.

Additional methods. Descriptions of gene construction, production and use of recombinant SFV, electrophysiology in organotypical rat hippocampal slices, flies and genetics, physiology and imaging in *Drosophila*, *in utero* electroporation and synthetic dye loading are available in **Supplementary Methods**.

Accession codes. GenBank: EU868624.

Note: Supplementary information is available on the Nature Methods website.

AUTHOR CONTRIBUTIONS
M.M. performed all molecular biology and spectroscopy to engineer TN-XXL; S.D. and V.S. performed electrophysiology in hippocampal slices; T.H., D.F.R. and A.B. imaged and evaluated TN-XXL in *Drosophila*; C.L. performed *in utero* electroporation; A.F.S., S.B.H., T.D.M.-F., T.B. and M.H. performed and evaluated experiments in mouse visual cortex; O.G., M.H., D.F.R., M.M. and A.F.S. wrote the manuscript; all authors contributed to editing the manuscript.

COMPETING INTERESTS STATEMENT
The authors declare competing financial interests: details accompany the full-text HTML version of the paper at http://www.nature.com/naturemethods/.

Published online at http://www.nature.com/naturemethods/
Reprints and permissions information is available online at
http://npg.nature.com/reprintsandpermissions/

1. Kerr, J.N.D. & Denk, W. Imaging *in vivo*: watching the brain in action. *Nat. Rev. Neurosci.* **9**, 195–205 (2008).
2. Stosiek, C., Garaschuk, O., Holthoff, K. & Konnerth, A. In vivo two-photon calcium imaging of neuronal networks. *Proc. Natl. Acad. Sci. USA* **100**, 7319–7324 (2003).
3. Kerr, J.N.D., Greenberg, D. & Helmchen, F. Imaging input and output of neocortical networks in vivo. *Proc. Natl. Acad. Sci. USA* **102**, 14063–14068 (2005).
4. Ohki, K., Chung, S., Ch'Ng, Y.H., Kara, P. & Reid, R.C. Functional imaging with cellular resolution reveals precise micro-architecture in visual cortex. *Nature* **433**, 597–603 (2005).
5. Ohki, K. *et al.* Highly ordered arrangement of single neurons in orientation pinwheels. *Nature* **442**, 925–928 (2006).
6. Mrsic-Flogel, T.D. *et al.* Homeostatic regulation of eye-specific responses in visual cortex during ocular dominance plasticity. *Neuron* **54**, 961–972 (2007).
7. Feldman, D.E. & Brecht, M. Map plasticity in somatosensory cortex. *Science* **310**, 810–815 (2005).
8. Hooks, B.M. & Chen, C.F. Critical periods in the visual system: changing views for a model of experience-dependent plasticity. *Neuron* **56**, 312–326 (2007).
9. Dombeck, D.A., Khabbaz, A.N., Collman, F., Adelman, T.L. & Tank, D.W. Imaging large-scale neural activity with cellular resolution in awake, mobile mice. *Neuron* **56**, 43–57 (2007).
10. Jackson, A. & Fetz, E.E. Compact movable microwire array for long-term chronic unit recording in cerebral cortex of primates. *J. Neurophysiol.* **98**, 3109–3118 (2007).
11. Miyawaki, A. Innovations in the imaging of brain functions using fluorescent proteins. *Neuron* **48**, 189–199 (2005).
12. Mank, M. & Griesbeck, O. Genetically encoded calcium indicators. *Chem. Rev.* **108**, 1550–1564 (2008).
13. Pologruto, T.A., Yasuda, R. & Svoboda, K. Monitoring neural activity and [Ca^{2+}] with genetically encoded Ca^{2+} indicators. *J. Neurosci.* **24**, 9572–9579 (2004).
14. Reiff, D.F. *et al.* In vivo performance of genetically encoded indicators of neural activity in flies. *J. Neurosci.* **25**, 4766–4778 (2005).
15. Mao, T., O'Connor, D.H., Scheuss, V., Nakai, J. & Svoboda, K. Characterization and subcellular targeting of GCaMP-type genetically encoded calcium indicators. *PLoS ONE* **3**, e1796 (2008).
16. Heim, N. & Griesbeck, O. Genetically encoded indicators of cellular calcium dynamics based on troponin C and green fluorescent protein. *J. Biol. Chem.* **279**, 14280–14286 (2004).
17. Mank, M. *et al.* A FRET-based calcium biosensor with fast signal kinetics and high fluorescence change. *Biophys. J.* **90**, 1790–1796 (2006).
18. Heim, N. *et al.* Improved calcium imaging in transgenic mice expressing a troponin C-based biosensor. *Nat. Methods* **4**, 127–129 (2007).

19. Potter, J.D. & Gergely, J. Calcium and magnesium binding-sites on troponin and their role in regulation of myofibrillar adenosine-triphosphatase. *J. Biol. Chem.* **250**, 4628–4633 (1975).
20. Filatov, V.L., Katrukha, A.G., Bulargina, T.V. & Gusev, N.B. Troponin: structure, properties, and mechanism of functioning. *Biochemistry (Mosc.)* **64**, 969–985 (1999).
21. DeMaria, C.D., Soong, T.W., Alseikhan, B.A., Alvania, R.S. & Yue, D.T. Calmodulin bifurcates the local Ca^{2+} signal that modulates P/Q-type Ca^{2+} channels. *Nature* **411**, 484–489 (2001).
22. Trigo-Gonzalez, G., Awang, G., Racher, K., Neden, K. & Borgford, T. Helix variants of troponin-C with tailored calcium affinities. *Biochemistry* **32**, 9826–9831 (1993).
23. Hendel, T. *et al.* Fluorescence change of genetic calcium indicators and OGB-1 correlated with neural activity and calcium in vivo and in vitro. *J. Neurosci.* **28**, 7399–7411 (2008).
24. Dräger, U.C. Receptive-fields of single cells and topography in mouse visual-cortex. *J. Comp. Neurol.* **160**, 269–289 (1975).
25. Trachtenberg, J.T. *et al.* Long-term *in vivo* imaging of experience-dependent synaptic plasticity in adult cortex. *Nature* **420**, 788–794 (2002).
26. Mandl, G., Desai, N. & Capaday, C. Nitrous-oxide modifies visual responses in the cat retina, striate cortex and superior colliculus. *Brain Res.* **193**, 401–414 (1980).
27. Emondi, A.A., Rebrik, S.P., Kurgansky, A.V. & Miller, K.D. Tracking neurons recorded from tetrodes across time. *J. Neurosci. Methods* **135**, 95–105 (2004).
28. Helmchen, F., Fee, M.S., Tank, D.W. & Denk, W. A miniature head-mounted two-photon microscope: high-resolution brain imaging in freely moving animals. *Neuron* **31**, 903–912 (2001).
29. Zipfel, W.R., Williams, R.M. & Webb, W.W. Non-linear magic: multiphoton microscopy in the biosciences. *Nat. Biotechnol.* **21**, 1369–1377 (2003).
30. Swindale, N.V., Grinvald, A. & Shmuel, A. The spatial pattern of response magnitude and selectivity for orientation and direction in cat visual cortex. *Cereb. Cortex.* **13**, 225–238 (2003).